Noise refocusing in a five-blade neutron interferometer

J. Nsofini, D. Sarenac, K. Ghofrani, M. G. Huber, M. Arif, D. G. Cory, and D. A. Pushin

Citation: Journal of Applied Physics **122**, 054501 (2017); doi: 10.1063/1.4996866
View online: https://doi.org/10.1063/1.4996866
View Table of Contents: http://aip.scitation.org/toc/jap/122/5
Published by the American Institute of Physics

Noise refocusing in a five-blade neutron interferometer

J. Nsofini,[1,2,a)] D. Sarenac,[1,2] K. Ghofrani,[2,3] M. G. Huber,[4] M. Arif,[4] D. G. Cory,[2,3,5,6] and D. A. Pushin[1,2]

[1]*Department of Physics, University of Waterloo, Waterloo, Ontario N2L3G1, Canada*
[2]*Institute for Quantum Computing, University of Waterloo, Waterloo, Ontario N2L3G1, Canada*
[3]*Department of Chemistry, University of Waterloo, Waterloo, Ontario N2L3G1, Canada*
[4]*National Institute of Standards and Technology, Gaithersburg, Maryland 20899, USA*
[5]*Perimeter Institute for Theoretical Physics, Waterloo, Ontario N2L2Y5, Canada*
[6]*Canadian Institute for Advanced Research, Toronto, Ontario M5G 1Z8, Canada*

(Received 18 April 2017; accepted 18 July 2017; published online 1 August 2017)

We provide a quantum information description of a proposed five-blade neutron interferometer geometry and show that it is robust against low-frequency mechanical vibrations and dephasing due to the dynamical phase. The extent to which the dynamical phase affects the contrast in a neutron interferometer is experimentally shown. In our model, we consider the coherent evolution of a neutron wavepacket in an interferometer crystal blade and simulate the effect of mechanical vibrations and momentum spread of the neutron through the interferometer. The standard three-blade neutron interferometer is shown to be immune to dynamical phase noise but prone to noise from mechanical vibrations, and the decoherence free subspace four-blade neutron interferometer is shown to be immune to mechanical vibration noise but prone to noise from the dynamical phase. Here, we propose a five-blade neutron interferometer and show that it is immune to both low-frequency mechanical vibration noise and dynamical phase noise. *Published by AIP Publishing.* [http://dx.doi.org/10.1063/1.4996866]

I. INTRODUCTION

Matter wave interferometry is a powerful and extremely sensitive tool to probe effects ranging from material properties to foundational physics.[1–5] For instance, neutron interferometry has been used to probe gravity, test quantum mechanics, perform phase imaging, and measure isotope-dependent nuclear scattering cross sections which are critical for interpreting material science scattering experiments.[6–10] Although high sensitivity and accuracy are achieved due to matter waves' small deBroglie wavelength and statistical inference, these massive particles couple to external degrees of freedom (DOF), leading to a loss of coherence. The loss of coherence as a result of non-refocused phases has been a subject of study in matter wave interferometry.[1,11–13] In this work, we specifically discuss concepts applied to a neutron interferometer (NI). However, they could easily applied to other matter wave interferometers. Isolation and control techniques have been developed to deal with some classes of noise,[14–17] but low-frequency vibrational noise still persists in these setups. The quest for noise-immune neutron interferometry motivated the design of the four-blade neutron interferometer with a decoherence free subspace (DFS),[18,19] which is robust to noise originating from mechanical vibration. Although the four-blade NI is robust against low-frequency vibrations, we will show that it is prone to dynamical phase noise.

During dynamical diffraction (DD) from a perfect crystal, a phase shift is introduced due to diffraction in the vicinity of the Bragg condition.[20–23] The so-called *dynamical phase* has tremendous angular sensitivity, which a recent experiment has measured to be about 30π rads per arcsec deviation from the Bragg angle in a silicon [220] crystal.[24] This sensitivity may offer a possibility of extracting fundamental quantities such as the neutron-electron scattering length, short-range gravitational interactions, and the Debye-Waller factor.[25–27]

The presence of the dynamical phase can lead to a reduction in the interferometry fringe visibility via a loss of coherence from a phase variation across the neutron beam.[1,28–30] As a result, it is desirable to remove the dynamical phase gradients. Such phases are naturally refocused in a three-blade NI but not the four-blade NI. Here, we propose a five-blade NI geometry that is robust to dynamical phase noise and also refocuses low frequency mechanical vibrational noise like the four-blade DFS NI.

This article is structured as follows: Sec. II gives a brief overview of the NI geometries considered including the proposed five-blade NI. In Sec. III, we give an analysis of the effect of the dynamical phase on the three-blade, four-blade, and five-blade neutron interferometers. The effect of external vibrations on each of the interferometer geometries is presented in Sec. IV, including a description of the noise in terms of the coherence function[1,31–33] to demonstrate the robustness of the five blade geometry to noise.

II. PERFECT CRYSTAL NEUTRON INTERFEROMETERS

A common NI geometry is the symmetric Laue-type which is machined from a perfect single crystal ingot of silicon and composed of several identical separate blades. A neutron incident on a blade in the NI is Bragg diffracted into

[a)]Electronic mail: jnsofini@uwaterloo.ca

two coherent beam paths. In this paper, we adopt the quantum operator formalism of Bragg diffraction from a perfect crystal.[34] The path degree of freedom (DOF) is a two-level system that is defined by the sign of the momentum in the y-direction (see Fig. 1 for the coordinate system); the path with $+k_y$ is labeled as path I and the path with $-k_y$ is labeled as path II. This two level system is isomorphic to a Bloch sphere.[35] The sign of the momentum is also used to label the detectors at the output such that I_O is identified with $+k_y$ and I_H is identified with $-k_y$. The labels are conventional.

The three-blade NI considered [see Fig. 1(a)] consists of three blades separated by the same distance ($2L$) in the Laue geometry. The second blade redirects the two paths to the third blade where they recombine and interfere. Each of the blades of the NI acts as a beam splitter. However, due to post selection on only those neutrons that reach the detector, the second blade actually implements a perfect π pulse. This enables a very simple and robust picture of the physics.

In the four-blade NI [Fig. 1(b)], the situation is similar to the three-blade NI with the difference that the two paths are redirected twice (with no mixing of states in the center of the interferometer) before reaching the last blade. This four-blade NI possess a DFS for low-frequency mechanical vibrational noise which significantly affects the three-blade NI.[18,19]

The proposed five-blade NI [Fig. 1(c)] can be thought of as two coupled Mach-Zehnder NIs. It is similar to the four-blade NI in that the neutrons are redirected twice but differs since the neutrons interfere on the additional blade in the middle.

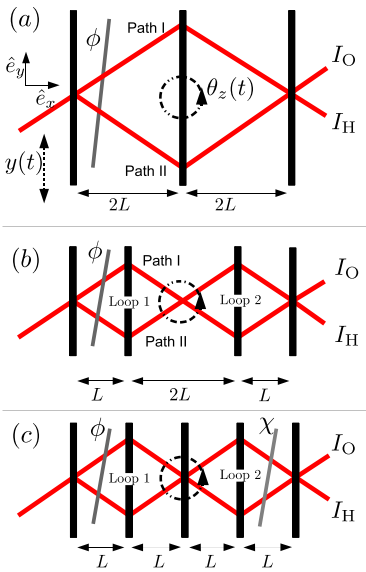

FIG. 1. Sketch of different NI geometries with phase flags producing phases ϕ and χ. The two detectors are the O-detector (I_O) and the H-detector (I_H). (a) A symmetric three-blade NI with phase flag ϕ and inter-blade distance $2L$. (b) Four-blade (DFS) NI with inter-blade distances: L, $2L$, L. (c) Five-blade (double loop Mach-Zehnder) NI with inter-blade distances L. The noise along the y-axis $y(t)$, and around the z-axis $\theta_z(t)$, is modeled as sinusoidal. I_{out}/I_{inc} is the ratio of the neutrons at the output $I_{out} = I_O + I_H$ to those at incidence I_{inc} when the beam splitters are assumed to be 50:50. $|\gamma_{MV}|$ and $|\gamma_{DD}|$ are the absolute values of the coherence function with z-noise ($\omega = 4.4$ Hz, see Fig. 8) and dynamical phase noise, each simulated for an interferometer with a blade thickness 0.9 mm and $L = 5$ cm. These dimensions are similar to those of the neutron interferometer in Ref. 19. In an ideal case, the absolute value of the coherence function is 1.

One figure of merit quantifying the quality of the interferometry setup is the fringe visibility or contrast. By introducing a phase difference between the two paths, the intensity at the exit oscillates between the intensities at the O-beam (I_O) and H-beam (I_H). From the intensity oscillations, the contrast is defined by

$$\mathcal{V} = \frac{I_{max} - I_{min}}{I_{max} + I_{min}}, \tag{1}$$

where I_{max} and I_{min} are the maximum and minimum intensities. Contrast is related to the coherence in the path DOF in an NI. Coherence refers to the ability of the two paths to interfere. It has been extensively studied in matter waves and photon optics.[32,33,36]

III. EFFECT OF THE DYNAMICAL PHASE

The beam splitting in each of the blades of the NI is governed by the theory of dynamical diffraction.[37] The theory of DD describes the interaction of matter waves and x-rays with a perfect crystal lattice when incident at the Bragg condition.[38–43] Perfect crystals coherently split a neutron beam into two components with properties defined by the periodicity of the crystal lattice and the energy of the neutron.[23,37] The mathematical formulation of the theory of DD is quite cumbersome, and we have shown recently that we may use a simplified quantum information approach.[34] Denoting the states corresponding to paths I and II as $|\mathrm{I}\rangle$ and $|\mathrm{II}\rangle$ and the operator of the blade as U_B, the states after the first blade of an NI is

$$U_B|\mathrm{I}\rangle = t|\mathrm{I}\rangle + r|\mathrm{II}\rangle, \quad U_B|\mathrm{II}\rangle = \bar{r}|\mathrm{I}\rangle + \bar{t}|\mathrm{II}\rangle, \tag{2}$$

where the transmission and reflection coefficients satisfy $|t|^2 + |r|^2 = 1$, and $\bar{r} = -r^*$, $\bar{t} = t^*$.

Due to symmetry, the Bragg diffraction is required to take the same form if the crystal is rotated by 180°. The crystal blade operator can be expressed as a composite sequence of rotations

$$U_B = R_z(\phi_t)R_{xy}(\phi_r, \alpha)R_z(\phi_t), \tag{3}$$

with the standard definitions of Bloch sphere rotations

$$R_z(\phi_t) = \exp\left(i\phi_t\sigma_z/2\right), \tag{4}$$

$$R_{xy}(\phi_r, \alpha) = \exp\left(i\alpha(\cos\left(\phi_r\right)\sigma_x + \sin\left(\phi_r\right)\sigma_y)/2\right), \tag{5}$$

where $\sigma_x = |\mathrm{I}\rangle\langle\mathrm{II}| + |\mathrm{II}\rangle\langle\mathrm{I}|$, $\sigma_y = -i|\mathrm{I}\rangle\langle\mathrm{II}| + i|\mathrm{II}\rangle\langle\mathrm{I}|$, $\sigma_z = |\mathrm{I}\rangle\langle\mathrm{I}| - |\mathrm{II}\rangle\langle\mathrm{II}|$ are the Pauli operators, $\phi_t = \arg[t]$, and $\phi_r = \arg[r]$. By definition, the dynamical phase is $\phi_t = \arg[t]$, while the phase between the two paths in an interferometer is $\beta = \phi_t - \phi_r$. Without the loss of generality, we will limit the R_{xy} rotation to be along σ_x, thereby effectively setting $\phi_r = 0$. This is justified because ϕ_r is a small linear contribution. This makes us to hypothesize a composite crystal blade operator:[34]

$$U_B = R_z(\beta)R_x(\alpha)R_z(\beta). \tag{6}$$

From these relations, one can identify the relation to the dynamical diffraction variables as

$$\beta = \arg[t], \quad t = \cos(\alpha/2), \quad \text{and} \quad r = \sin(\alpha/2), \tag{7}$$

with $\alpha \in [0, \pi]$. When $\alpha = \pi/2$, the blade acts as a 50:50 beam splitter.

We will now apply the Bloch sphere rotation formalism described above to the three NI geometries to analyse the relevance of the dynamical phase in each case.

A. Three-blade Mach-Zehnder neutron interferometer

In the three-blade NI, the first and last blades each act as a composite rotation $U_B = R_z(\beta)R_x(\alpha)R_z(\beta)$. The middle blade serves as a mirror to redirect the two paths onto the third blade and hence is properly represented by $U_M = R_z(\beta)$ $R_x(\pi)R_z(\beta) = R_x(\pi)$. With a phase difference ϕ (due to the phase flag) between path I and path II of the three-blade NI [Fig. 1(a)], the overall operation sequence is

$$\begin{aligned} R_3 &= U_B U_M R_z(\phi) U_B, \\ &= R_z(\beta)R_x(\alpha)R_z(\beta)R_x(\pi)R_z(\phi)R_z(\beta)R_x(\alpha)R_z(\beta), \\ &= R_z(\beta)R_x(\alpha)R_x(\pi)R_z(\phi)R_x(\alpha)R_z(\beta), \end{aligned} \tag{8}$$

where the identity $R_x(\pi) = R_z(\beta)R_x(\pi)R_z(\beta)$ was used in the second line. The first and last $R_z(\beta)$ rotations can be ignored since the incoming beam is an eigenstate of σ_z and the measurement is done along the z-basis. With an initial state $|\mathrm{I}\rangle$, the intensities of neutrons at the O-detector and H-detector for $\alpha = \pi/2$ are

$$I_{O3}(\phi) = \frac{1}{2}(1 + \cos\phi), \tag{9}$$

$$I_{H3}(\phi) = \frac{1}{2}(1 - \cos\phi). \tag{10}$$

The three-blade NI is therefore immune to dynamical noise as β is refocused. It is worth noting that the resulting operation of the three-blade NI is analogous to the Hahn echo sequence.[44]

B. Four-blade neutron interferometer

In the four-blade NI, the operator of the first and fourth blades is U_B and that of the second and third blades is U_M. With the initial state $|\mathrm{I}\rangle$ and a phase difference ϕ between paths I and II [see Fig. 1(b)], the overall operator sequence for the four-blade NI is

$$\begin{aligned} R_4 &= U_B R_x(\pi)R_x(\pi)R_z(\phi)U_B \\ &= R_z(\beta)R_x(\alpha)R_z(2\beta)R_z(\phi)R_x(\alpha)R_z(\beta). \end{aligned} \tag{11}$$

The identity $\mathbb{I} = R_x(\pi)_x R(\pi)$ was used in the second line. In the case where $\alpha = \pi/2$, the intensities at the O-beam and H-beam are given by

$$I_{O4}(\phi) = \frac{1}{2}[1 - \cos(\phi + 2\beta)],$$

$$I_{H4}(\phi) = \frac{1}{2}[1 + \cos(\phi + 2\beta)].$$

The presence of β in the intensity implies that the dynamical phase is not refocused in the four-blade NI. Upon averaging over neutrons with different momenta arriving at the detector, dephasing occurs in a four-blade NI. The dephasing causes a reduction in the coherence and hence the contrast. The loss in contrast depends on the noise spectrum of β. The average neutron intensity at the detectors is

$$\overline{I_{O4}}(\phi) = \frac{1}{2}\left[1 - \int d\beta p(\beta)\cos(\phi + 2\beta)\right], \tag{12}$$

$$\overline{I_{H4}}(\phi) = \frac{1}{2}\left[1 + \int d\beta p(\beta)\cos(\phi + 2\beta)\right], \tag{13}$$

where $p(\beta)$ is the probability density function. The effect of this dynamical phase was pointed out in early works on neutron interferometry,[29,45] but the extent to which it affects the coherence in a four-blade NI is not well quantified experimentally. The intensity can be re-written as

$$\overline{I_{O4}}(\phi) = \frac{1}{2}\left[1 - |\gamma|\cos\left(\phi + \arg[\gamma]\right)\right], \tag{14}$$

$$\overline{I_{H4}}(\phi) = \frac{1}{2}\left[1 + |\gamma|\cos\left(\phi + \arg[\gamma]\right)\right], \tag{15}$$

where

$$\gamma = \int d\beta\, p(\beta) e^{i2\beta} \tag{16}$$

is the coherence function. The presence of a phase distribution leads to a reduction in coherence and hence the contrast. This loss of contrast is usually small since the width of the distribution accepted by the NI crystal (Darwin width) is very narrow ($\sim 10^{-6}$ rad), thereby limiting the strength of the noise.

In an experiment to measure the neutron charge radius, the dynamical phase was measured as the extent to which the contrast is affected by the dynamical phase. In the experiment, a perfect Si crystal blade of thickness 2 mm and the crystallographic orientation [111] was added after the first blade of a three-blade NI.[26,46] When the crystal is aligned to the Bragg angle of the interferometer and the Bragg reflected beams are blocked, it replicates the dynamical phase that manifests itself in a four-blade NI. Using $\alpha = \pi/2$, the normalized output intensity at the O-beam in this case is similar to Eq. (14) and can be expressed as follows:

$$\overline{I_O}(\phi) = \mathcal{A}_\mathrm{O} - |\mathcal{B}_O|\cos(\phi + \arg[\mathcal{B}_O]), \tag{17}$$

where as shown in[23]

$$\mathcal{A}_O = \int d\delta\theta\, g(\delta\theta), \quad \mathcal{B}_O = \int d\delta\theta\, g(\delta\theta) e^{i\beta}, \tag{18}$$

$$g(\delta\theta) = \frac{\sigma_\theta/\pi}{\sigma_\theta^2 + (\delta\theta - \delta\theta_0)^2}. \tag{19}$$

The average here is taken over $\delta\theta = \theta - \theta_B$ since $\beta = \beta(\delta\theta)$ is a function of the angular deviation, where θ_B is the Bragg angle. The measured contrast and phase against $\delta\theta$ are shown

in Figs. 2(a) and 2(b), respectively. Also shown is the simulated momentum distribution $g(\delta\theta)$ accepted by a single crystal, where the full width at half maximum (FWHM) is given by the Darwin width of the crystal $\sigma_\theta = 4.26$ μrad. The addition of an extra blade breaks the blade separation symmetry (equal separation between all the blades). The result of this is that the measured phase depicted in Fig. 2(b) is composed of the dynamical phase and the phase due to defocussing. By separating these two phases, we extract a purely dynamical phase given by Fig. 3. This is achieved by using the FWHM extracted from the experiments and assuming that that momentum distribution only changes when the orientation of the crystal changes and not due to defocussing. A similar experiment has been done with the extra crystal blade oriented in the Bragg geometry.[23] By accounting for this dynamical phase, we can estimate the maximum contrast of the four-blade NI. If the four-blade NI is made from 1 mm thick Si blades in the (111) crystallographic orientation (as per Ref. 19) and illuminated with neutrons of $\lambda = 2.71$ Å, the estimated maximum contrast is ~85%.

C. Five-blade double loop neutron interferometer

The five-blade NI is similar to the four-blade NI but with an additional middle blade U_B. With a phase ϕ in the first loop and χ in the second loop [see Fig. 1(c)], the combined operation of the interferometer is

$$\begin{aligned} R_5 &= U_B R_x(\pi) U_B R_x(\pi) R_z(\phi) U_B \\ &= R_z(\beta) R_x(\alpha) R_z(\chi) R_x(\alpha) R_z(\phi) R_x(\alpha) R_z(\beta). \end{aligned}$$

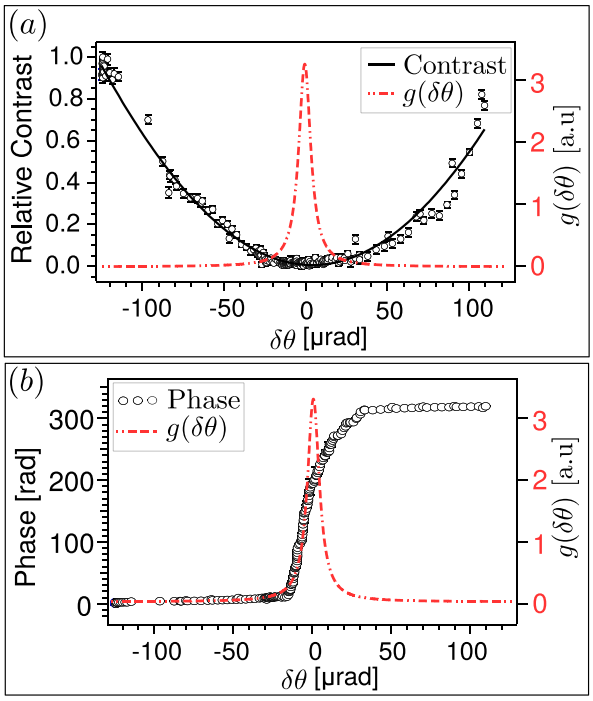

FIG. 2. Measured effect of the dynamical phase on contrast.[46] A 2 mm thick (111) Si crystal is added after the first blade of a three-blade neutron interferometer and rotated around the Bragg angle. (a) The contrast and momentum distribution $g(\delta\theta)$ plotted against the Si blade rotation $\delta\theta$. (b) The dynamical phase and the simulated momentum distribution $g(\delta\theta)$ plotted against the Si blade rotation $\delta\theta$. The full width at half maximum of the momentum distribution is equal to the Darwin width of the crystal $\sigma_D = 4.26$ μrad.

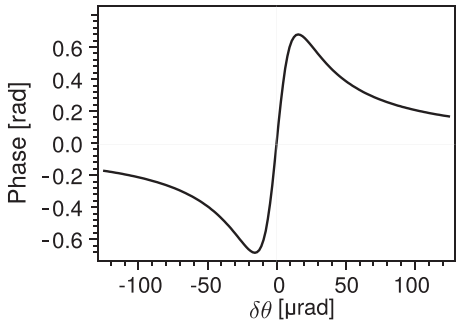

FIG. 3. The dynamical phase separated from the total phase shown in Fig. 2(b).

With an incident state of $|\mathrm{I}\rangle$ onto the NI, the intensity at the O- and H-beams is

$$I_{O5}(\phi,\chi) = \frac{1}{4}[2 + \cos(\chi - \phi) - \cos(\chi + \phi)], \tag{20}$$

$$I_{H5}(\phi,\chi) = \frac{1}{4}[2 - \cos(\chi - \phi) + \cos(\chi + \phi)]. \tag{21}$$

Notice that there is no dependence on β and so the dynamical phase is refocused. The refocusing of the dynamical phase can also be understood in the sense of chirping, as the wavevectors that were travelling faster than the mean wavevector before the second blade (which acts as a mirror) tend to travel slower than the mean wavevector after the mirror blade (and vice-versa). This is the same principle of noise refocusing, which is employed in nuclear magnetic resonance.[44,47,48]

We conclude that the three-blade and five-blade NIs are immune to dynamical phase noise originating from the momentum spread of the incoming neutrons, while the four-blade NI is not. Next, we will analyse and compare the performance of these interferometers against external vibrational noise.

IV. EFFECTS OF MECHANICAL VIBRATION

The effect of mechanical vibrations on matter wave interferometry has been studied for specific implementations.[49] In neutron interferometry, mechanical vibrations are commonly reduced by using vibration isolation systems although the effect of low-frequency vibration still persists. The four-blade NI has the experimentally demonstrated advantage over the three-blade NI of being robust against slow varying external mechanical vibrational noise.[19] In this article, we adopt the vibration model in Ref. 18, which treats vibrations as sinusoidal oscillations in the form $\zeta(t) = \zeta_0 \sin(\omega t + \varphi)$, where ζ_0 is the amplitude of the noise, ω is the frequency, and $\varphi \in [0, 2\pi]$ is a random phase that considers different arrival times of the neutrons at the first blade. Mechanical vibrations may change the momentum of the neutron, which leads to a phase difference around any closed interferometry loop

$$\Delta\Phi = \frac{1}{\hbar}\int_{\text{path I}} \vec{p}_{\mathrm{I}} \cdot d\vec{s} - \frac{1}{\hbar}\int_{\text{path II}} \vec{p}_{\mathrm{II}} \cdot d\vec{s} = \frac{1}{\hbar}\oint \Delta\vec{p} \cdot d\vec{s},$$

where $\vec{p}_{\mathrm{I}}$ and $\vec{p}_{\mathrm{II}}$ are associated momentum changes for path I and path II, respectively, and $\Delta\vec{p} = \vec{p}_{\mathrm{I}} - \vec{p}_{\mathrm{II}}$. The main contributions to the decrease in coherence come from the translational vibration noise along the y-axis (y-noise) and rotation vibration around the z-axis (θ_z referred to simply as z-noise). The y-noise comes from the interferometer vibrations along the reciprocal lattice vector and the z-noise from rotations around the axis perpendicular to the plane of interference. Using the form of the noise stated above, the y-noise is modelled as $y(t) = y_0 \sin(\omega t + \varphi)$ and the z-noise as $\theta(t) = \theta_0 \sin(\omega t + \varphi)$. The frequency of the noise along the y-axis and the z-axis is not necessarily the same.

A. Y-noise

Let the velocity of the incidence neutron be decomposed into two components, perpendicular and parallel to the reciprocal lattice vector $v = v_\perp \hat{e}_x + v_\parallel \hat{e}_y$. If the interaction of the neutron with the blade is modelled as a bouncing ball from a hard surface, the velocity along the x-axis is not affected while that along the y-axis is $v_y = -v_\parallel + 2u_y(t)$, where $u_y(t) = dy(t)/dt$ is the time derivative. Assuming the neutron enters the interferometer at $t = 0$, the phase shift between path I and path II caused by y-noise vibrations in a three blade NI is

$$\Delta\Phi(\varphi) = \frac{32m}{\hbar}\tau^2\left[v_\parallel - u_y(0)\right]\dot{u}_y(0), \tag{22}$$

where m is the mass of the neutron, $\tau = L/v_\perp$, and L is the distance between the first and second blades of the interferometer. For low-frequency noise where $\omega\tau \ll 1$,

$$\Delta\Phi(\varphi) = \frac{32mv_y y_0 \tau^2}{\hbar}\omega^2 \sin\varphi, \tag{23}$$

since $v_y \gg u_y(0)$. The probability of detecting a single neutron at the O- and H-detectors in the three-blade NI is

$$I_{O3}(\phi) = \frac{1}{2}\left[1 + \cos\left(\phi + \Delta\Phi(\varphi)\right)\right], \tag{24}$$

$$I_{H3}(\phi) = \frac{1}{2}\left[1 - \cos\left(\phi + \Delta\Phi(\varphi)\right)\right]. \tag{25}$$

Each neutron arrives at the first blade at different instances and picks a different initial phase φ. Integrating over a uniform probability distribution $p(\varphi) = 1/2\pi$, the average intensity at the O-beam is

$$\overline{I_{O3}}(\phi) = \frac{1}{2}\left[1 + |\gamma|\cos\left(\phi + \arg[\gamma]\right)\right], \tag{26}$$

where γ is the coherence function which is defined as for statistically stable noise[33,50]

$$\gamma = \frac{1}{2\pi}\int_0^{2\pi} \exp\left[i\Delta\Phi(\varphi)\right]d\varphi. \tag{27}$$

The absolute value of the coherence function, $|\gamma|$, for the three-blade NI is equal to the contrast $\mathcal{V}$ defined in Eq. (1). We consider an interferometer with $L = 5$ cm, a wavelength of 4.4 Å, and a y-noise with an amplitude of $y_0 = 0.1\ \mu$m. Using these values, the coherence function for the y-noise in the three-blade NI reduces to

$$\gamma = J_0(\Omega\omega^2), \quad \text{with} \quad \Omega = \frac{32mv_y y_0\tau^2}{\hbar}, \tag{28}$$

where J_0 is the Bessel function of the first kind. Shown in Fig. 4 is $\mathcal{V} = |\gamma|$ vs the noise strength ω, where it can be compared to the four-blade and five-blade NIs.

In the four-blade NI, the phase difference in the first loop $\Delta\Phi_1$ and the phase differences in the second loop $\Delta\Phi_2$ (see 1b for the loop labels) are

$$\Delta\Phi_1 = -\frac{4m\tau^2}{\hbar}\left[v_\parallel - u_y(0)\right]\left[2\dot{u}_y(0) + \tau\ddot{u}_y(0)\right], \tag{29}$$

$$\Delta\Phi_2 = \frac{4m\tau^2}{\hbar}\left[v_\parallel - u_y(0)\right]\left[2\dot{u}_y(0) + 7\tau\ddot{u}_y(0)\right]. \tag{30}$$

The phase difference is effectively the sum of the phases in loops 1 and 2, and for low-frequency noise where $\omega\tau \ll 1$, the phase difference is given by

$$\Delta\Phi(\varphi) = \frac{24mv_y y_0\tau^3}{\hbar}\omega^3\cos\varphi. \tag{31}$$

The probability of detecting a single neutron at the O- and H- detectors in the four-blade NI is

$$I_{O4}(\phi) = \frac{1}{2}\left[1 - \cos\left(\phi + \Delta\Phi(\varphi)\right)\right], \tag{32}$$

$$I_{H4}(\phi) = \frac{1}{2}\left[1 + \cos\left(\phi + \Delta\Phi(\varphi)\right)\right]. \tag{33}$$

Taking the average over the uniform phase distribution of φ and considering the H-beam in the DFS as it carries the same phase information as the O-beam in the three-blade NI, the intensity of the DFS is

$$\overline{I_{H4}}(\phi) = \frac{1}{2}(1 + \gamma\cos\phi). \tag{34}$$

where the coherence similar to the one for the three-blade NI is

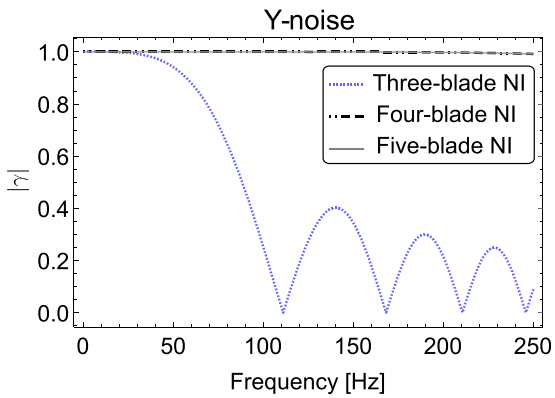

FIG. 4. Simulations of the variation of the absolute value of the coherence function γ versus strength ω for each of the three-, four-, and five-blade neutron interferometers. The coherence of the four- and five-blade NI is not affected for low frequencies although they are affected at frequencies of $\omega > 250$ Hz. Note that the decoherence free condition from the configuration where $\phi = -\chi + \pi$ is used.

$$\gamma = J_0(\Omega\omega^3), \quad \text{with} \quad \Omega = \frac{24mv_y y_0\tau^3}{\hbar}. \tag{35}$$

The coherence function $|\gamma| = \mathcal{V}$ for the four-blade NI under the influence of y-noise is compared to the three-blade and five-blade NIs in Fig. 4.

In the five-blade NI, we first resolve the path taken by the neutron to the last blade into four trajectories. For simplicity, we split the four trajectories into two categories, the *symmetric* case and the *antisymmetric* case. The symmetric case contains the two paths corresponding to the middle blade acting as a perfect transmitter [$|\mathrm{I}\rangle \rightarrow |\mathrm{I}\rangle$ and $|\mathrm{II}\rangle \rightarrow |\mathrm{II}\rangle$, see Fig. 5(a)], and the antisymmetric case is where the middle blade acts as a perfect reflector [$|\mathrm{I}\rangle \rightarrow |\mathrm{II}\rangle$ and $|\mathrm{II}\rangle \rightarrow |\mathrm{I}\rangle$, see Fig. 5(b)]. The symmetric case is identical to the four-blade NI. In a similar way, we split the total phase into two components. In the symmetric case, the phases denoted by $\Delta\Phi_1$ and $\Delta\Phi_2$ for loop 1 and loop 2, respectively, are

$$\Delta\Phi_1 = -\frac{4m\tau^2}{\hbar}\left[v_\parallel - u_y(0)\right]\left[2\dot{u}_y(0) + \tau\ddot{u}_y(0)\right], \tag{36}$$

$$\Delta\Phi_2 = \frac{4m\tau^2}{\hbar}\left[v_\parallel - u_y(0)\right]\left[2\dot{u}_y(0) + 7\tau\ddot{u}_y(0)\right]. \tag{37}$$

In the antisymmetric case, the phases in loop 1 and 2 denoted by $\Delta\Phi'_1$ and $\Delta\Phi'_2$ respectively are

$$\Delta\Phi'_1 = \Delta\Phi_1, \tag{38}$$

$$\Delta\Phi'_2 = -\frac{4m\tau^2}{\hbar}\left[v_\parallel - u_y(0)\right]\left[2u_y(0) + 3\tau\ddot{u}_y(0)\right]. \tag{39}$$

In the low-frequency noise regime where $\tau\omega \ll 1$, the resulting phase difference in the symmetric case and the antisymmetric case is

$$\Delta\Phi(\varphi) = \frac{24mv_\parallel y_0\tau^3}{\hbar}\omega^3\cos\varphi, \quad \text{symmetric}, \tag{40}$$

$$\Delta\Phi'(\varphi) = \frac{16mv_\parallel y_0\tau^2}{\hbar}\omega^2\sin\varphi, \quad \text{antisymmetric}. \tag{41}$$

The phase difference from external vibrations along the y-axis cancels out in the symmetric case but effectively doubles in the anti-symmetric loop. The effect of this noise and conditions under which it can be removed will be discussed later. Prior to this, we examine the effect of y-noise.

With a phase ϕ in the first loop and χ in the second loop [see Fig. 1(c)], the probability of detecting a single neutron at the O- and H- detectors of the five-blade NI is

$$I_{O5}(\phi,\chi) = \frac{1}{4}\big(2 + \cos\left[\chi - \phi + \Delta\Phi(\varphi)\right] - \cos\left[\chi + \phi + \Delta\Phi'(\varphi)\right]\big), \tag{42}$$

$$I_{H5}(\phi,\chi) = \frac{1}{4}\big(2 - \cos\left[\chi - \phi + \Delta\Phi(\varphi)\right] + \cos\left[\chi + \phi + \Delta\Phi'(\varphi)\right]\big), \tag{43}$$

where the symmetric $\Delta\Phi(\varphi)$ and the antisymmetric phase differences are defined in Eqs. (40) and (41). The average H-beam intensity over the uniform distribution of φ of the H-beam is

$$\overline{I_{H5}}(\phi,\chi) = \frac{1}{4}\big(2 - |\gamma|\cos\left(\chi - \phi + \arg\gamma\right) + |\gamma'|\cos\left(\chi + \phi + \arg\gamma'\right)\big). \tag{44}$$

With the coherence function of the symmetric and antisymmetric cases, we get

$$\gamma = \frac{1}{2\pi}\int_0^{2\pi}\exp\left[i\Delta\Phi(\varphi)\right]d\varphi, \qquad \gamma' = \frac{1}{2\pi}\int_0^{2\pi}\exp\left[i\Delta\Phi'(\varphi)\right]d\varphi. \tag{45}$$

For y-noise, it can be shown that

$$\gamma = J_0(\Omega\omega^3), \quad \text{with} \quad \Omega = \frac{24mv_\parallel y_0\tau^3}{\hbar}, \tag{46}$$

$$\gamma' = J_0(\Omega'\omega^2), \quad \text{with} \quad \Omega' = \frac{16mv_\parallel y_0\tau^2}{\hbar}. \tag{47}$$

Consider an interferometer where the amplitude of y-noise is $y_0 = 0.1\,\mu$m. The H-beam intensity without noise ($\omega = 0$) is presented in Fig. 6(a). In Figs. 6(b), 6(c), and 6(d), the same intensity is plotted for y-noise with $\omega = 150$ Hz, $\omega = 200$ Hz, and $\omega = 250$, respectively. The region through the density plots where the oscillations are dampened illustrates the effect of noise. It is clearly visible in the plot that there are some combinations of the phase on the first and second loops for which the effect of noise is minimal. One obvious choice from Fig. 6(b) is the vertical line $\phi = \pi$; however, this line is only unique for $\omega = 200$ Hz. For a different ω, a different vertical line would be required. On the other hand, the set of conditions which include the lines $\phi = -\chi + \mu$, where μ is a constant, is capable of refocusing any low-frequency mechanical vibrational noise. Along these lines, the effect of noise results in a phase independent shift of the intensity profile, which has no effect on the coherence.

By choosing $\mu = \pi$ to get $\chi = \pi - \phi$, the intensity in the presence of y-noise can be expressed as

$$\overline{I_{H5}}(\phi,\pi-\phi) = \frac{1}{4}\left[2 - \gamma' - |\gamma|\sin\left(2\phi + \arg(\gamma)\right)\right]. \tag{48}$$

In the five-blade NI, noise acts as a phase independent shift or an additional background contribution of $1 - \gamma'$. As shown

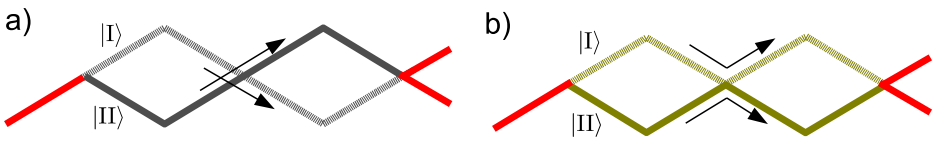

FIG. 5. The five-blade interferometer split into to four paths which constitute two cases. (a) Symmetric case: $|\mathrm{I}\rangle \rightarrow |\mathrm{I}\rangle$ and $|\mathrm{II}\rangle \rightarrow |\mathrm{II}\rangle$. (b) Anti-symmetric case: $|\mathrm{I}\rangle \rightarrow |\mathrm{II}\rangle$ and $|\mathrm{II}\rangle \rightarrow |\mathrm{I}\rangle$.

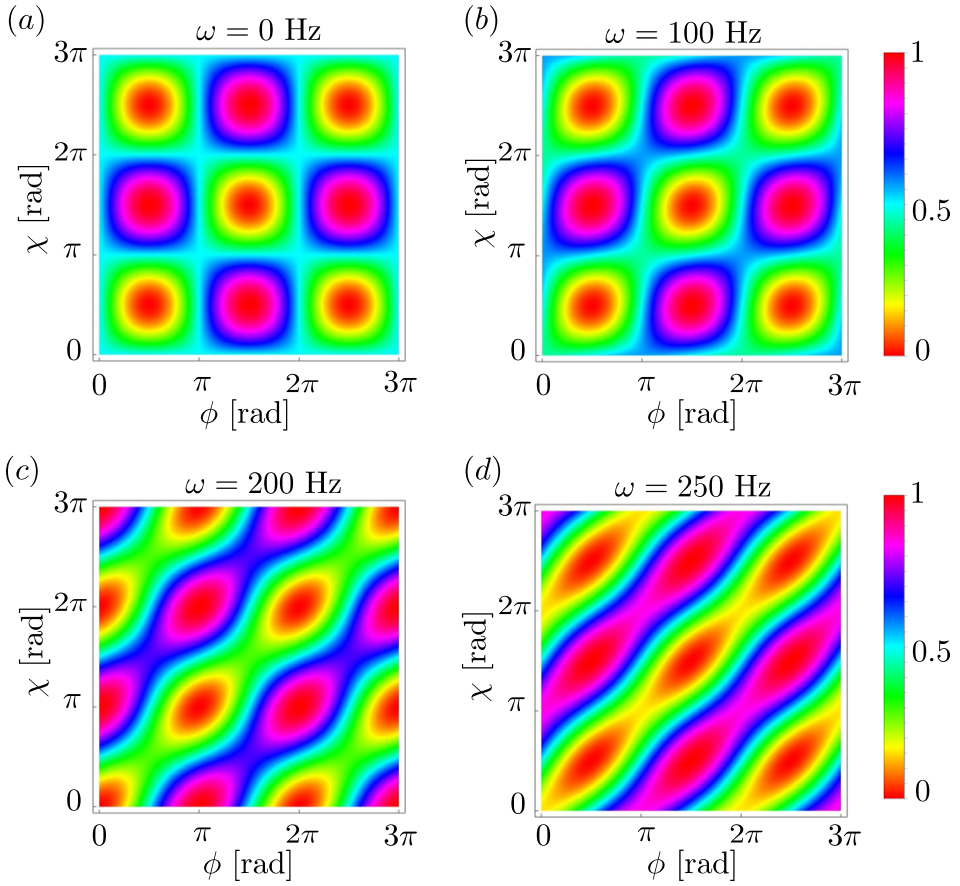

FIG. 6. Density plot of the intensity at the H-beam for a five blade-neutron neutron interferometer as a function of the phase, ϕ, in loop 1, and phase, χ, in loop 2. (a) The intensity without noise. In this plot, the oscillations are clearly visible along any line in the 2D plane (ϕ, χ). The intensity in the presence of y-noise is shown in (b) with $\omega = 100$ Hz, in (c) with $\omega = 200$ Hz, and in (d) for $\omega = 250$ Hz. The interference pattern is dampened along some configurations of ϕ and χ; for example, $\chi = \phi +$ constant. In the simulation, the interferometer separation between blades is $L = 5$ cm and the neutron wavelength is 4.4 Å.

in Fig. 7, the interference pattern is displaced along the vertical axis as the noise frequency, ω, is increased. Even though, the coherence, or the depth of the modulation, $|\gamma|$ remains the same, the contrast as defined by Eq. (1) reduces. For a y-noise of 100 Hz, the interferogram is offset by 0.2 which results in a relative contrast of about 82%. In Fig. 4, a plot of $|\gamma|$ for the five-blade NI is compared with that for the three and four blade NIs. Therefore, the five-blade NI is capable of refocusing low-frequency noise just as the four-blade DFS NI. The coherence of the four-blade and five-blade NIs is not noticeably affected at low frequencies although they start to get affected at frequencies above 250 Hz.

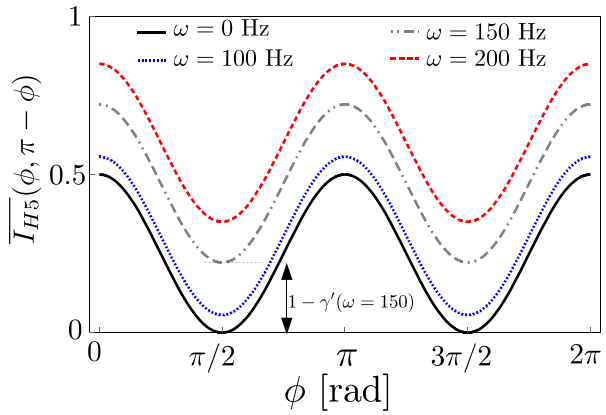

FIG. 7. The H-beam intensity as a function of the correlated phase ϕ for low-frequency y-noise with $\omega = 0$, 100, 150, and 200 Hz. When the noise refocusing condition $\phi + \chi = \pi$ is used, the effect of noise is simply an additional background term, with a magnitude of $1 - \gamma'$.

B. Z-noise

The noise around the z-axis is modeled as $\theta(t) = \theta_0 \sin(\omega t + \varphi)$. Again assuming an incident neutron on the first blade at $t = 0$ and using small angle approximations, the phase difference for a three-blade NI is

$$\Delta\Phi(\varphi) = \frac{32m\tau}{\hbar}\left[v_\parallel - 2L\dot{\theta}(0)\right]L\dot{\theta}(0), \tag{49}$$

$$= \frac{32mv_\perp v_\parallel \theta_0 \tau^2}{\hbar}\omega\cos\varphi. \tag{50}$$

In the four-blade NI, the phase differences, $\Delta\Phi_1$, in loop 1 and, $\Delta\Phi_2$, in loop 2 are given by

$$\Delta\Phi_1 = \frac{8m\tau}{\hbar}\left[v_\parallel - 2L\dot{\theta}(0)\right]\left[L\dot{\theta}(0) - L\tau\ddot{\theta}(0)\right], \tag{51}$$

$$\Delta\Phi_2 = -\frac{8m\tau}{\hbar}\left[v_\parallel - 2L\dot{\theta}(0)\right]\left[L\dot{\theta}(0) + 5L\tau\ddot{\theta}(0)\right], \tag{52}$$

such that the low-frequency phase difference is

$$\Delta\varphi = -\frac{48mv_\perp v_\parallel \theta_0 \tau^3}{\hbar}\omega^2\sin\varphi. \tag{53}$$

The phase difference for the five-blade NI is again split into two components. The symmetric phase differences acquired in loop one $\Delta\Phi_1$ and loop two $\Delta\Phi_2$ are

$$\Delta\Phi_1 = \frac{8m\tau}{\hbar}\left[v_\parallel - 2L\dot{\theta}(0)\right]\left[L\dot{\theta}(0) - L\tau\ddot{\theta}(0)\right], \tag{54}$$

$$\Delta\Phi_2 = -\frac{8m\tau}{\hbar}\left[v_{\parallel} - 2L\dot{\theta}(0)\right]\left[L\dot{\theta}(0) + 5L\tau\ddot{\theta}(0)\right], \quad (55)$$

and the phases of loop 1 and loop 2 in the antisymmetric case are

$$\Delta\Phi_1' = \Delta\Phi_1, \quad (56)$$

$$\Delta\Phi_2' = \frac{8m\tau}{\hbar}\left[v_{\parallel} - 2L\dot{\theta}(0)\right]\left[L\dot{\theta}(0) + L\tau\ddot{\theta}(0)\right]. \quad (57)$$

For low-frequency noise where $\tau\omega \ll 1$, the phase differences in the symmetric case and the antisymmetric case are

$$\Delta\Phi(\varphi) = -\frac{48mv_{\perp}v_{\parallel}\theta_0\tau^3}{\hbar}\omega^2\sin\varphi, \quad \text{symmetric}, \quad (58)$$

$$\Delta\Phi'(\varphi) = \frac{16mv_{\perp}v_{\parallel}\theta_0\tau^2}{\hbar}\omega\sin\varphi, \quad \text{antisymmetric}. \quad (59)$$

Just like the y-noise, the phase difference from external vibrations along the z-axis cancels out in the symmetric but effectively doubles in the anti-symmetric case. The effect of this noise and conditions under which it can be removed is similar that of the y-noise.

The coherence function can be calculated for the z-noise just as was done for the y-noise. The absolute value of the coherence function γ with frequency ω for vibrations around the z-axis is show in Fig. 8. The vibration amplitude is $\theta_0 = 0.1$ μrad, with other conditions maintained as for the y-noise. The coherence function of the four-blade and five-blade interferometers remains unchanged at higher frequencies where the three-blade NI is significantly affected for noise with frequencies greater than 4 Hz.

It is worth noting here that the noise refocusing strength of the five-blade NI goes beyond the symmetric noise that is refocused by the four blade neutron interferometer. If the noise is antisymmetric, the five-blade NI still retains the ability to refocus but with the configuration changed to $\phi = \chi + \mu$. The four-blade DFS NI does not have the ability to refocus this class of noise.

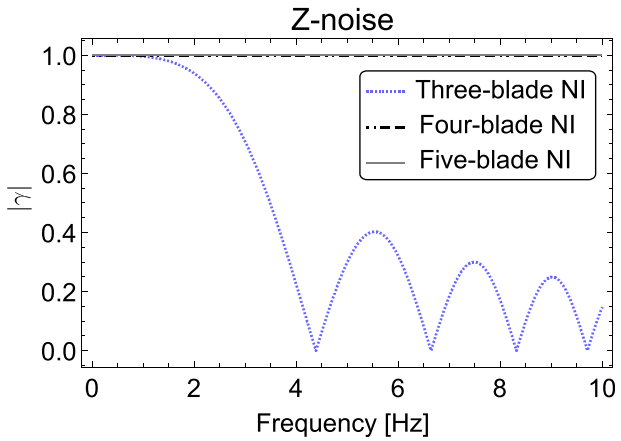

FIG. 8. Simulations of the variation of the absolute value of the coherence function with z-noise strength for each of the various neutron interferometers. The coherence function of the four-blade and five-blade interferometers remains unchanged at frequencies greater than 4 Hz, while the three-blade NI is significantly affected. Note that the decoherence free condition from the configuration of the phase flags $\phi = -\chi + \pi$ is used.

V. CONCLUSION

We formulated the action of the NI blade as a composite unitary operator and used it to study how the dynamical phase affects the performance of different neutron interferometer geometries. We showed that this noise is refocused in a proposed five-blade neutron interferometer, which is also insensitive to both dynamical and low frequency vibration noises. The power of the five-blade neutron interferometer includes that it can also refocus antisymmetric noise. This class of noise could originate from various gradients (i.e., magnetic and temperature). From the analyses, we have a theory that can be generalized to any interferometer geometry to understand noise effects. The concepts presented here can be adapted to other matter-wave interferometers. Similar quantities related to the coherence can be extracted from various quantum systems in order to characterize noise.[51] Our future plan is to test these concepts experimentally.

ACKNOWLEDGMENTS

This work was supported by the Canada Excellence Research Chairs (CERC) program (215284), the Natural Sciences and Engineering Research Council of Canada (NSERC) Discovery program, Collaborative Research and Training Experience (CREATE) program, and the Canada First Research Excellence Fund (CFREF). M. Huber would like to thank Fred E. Wietfeldt for useful discussions and to appreciate the support of the National Science Foundation (NSF PHY-0245679).

[1]H. Rauch and S. Werner, *Neutron Interferometry: Lesson in Experimental Quantum Mechanics* (Clarendon Press, Oxford, 2000).
[2]A. D. Cronin, J. Schmiedmayer, and D. E. Pritchard, Rev. Mod. Phys. **81**, 1051 (2009).
[3]K. Li, M. Arif, D. Cory, R. Haun, B. Heacock, M. Huber, J. Nsofini, D. Pushin, P. Saggu, D. Sarenac *et al.*, Phys. Rev. D **93**, 062001 (2016).
[4]D. Sarenac, M. G. Huber, B. Heacock, M. Arif, C. W. Clark, D. G. Cory, C. B. Shahi, and D. A. Pushin, Opt. Express **24**, 22528 (2016).
[5]C. W. Clark, R. Barankov, M. G. Huber, M. Arif, D. G. Cory, and D. A. Pushin, Nature **525**, 504 (2015).
[6]S. A. Werner, J. L. Staudenmann, and R. Colella, Phys. Rev. Lett. **42**, 1103 (1979).
[7]K. C. Littrell, B. E. Allman, and S. A. Werner, Phys. Rev. A **56**, 1767 (1997).
[8]M. Schlenker, W. Bauspiess, W. Graeff, U. Bonse, and H. Rauch, J. Magn. Magn. Mater. **15**, 1507 (1980).
[9]M. Zawisky, U. Bonse, F. Dubus, Z. Hradil, and J. Rehacek, Europhys. Lett. **68**, 337 (2004).
[10]P. Huffman, M. Arif, T. Black, D. Jacobson, K. Schoen, W. Snow, and S. Werner, in *Proceedings of the Eighth International Conference on Neutron Scattering* [Physica B **385–386**(2), 1365 (2006)].
[11]M. Sudo, *Quantum Interferometry in Phase Space* (Springer, 2006).
[12]D. Hellweg, L. Cacciapuoti, M. Kottke, T. Schulte, K. Sengstock, W. Ertmer, and J. J. Arlt, Phys. Rev. Lett. **91**, 010406 (2003).
[13]F. Marquardt and C. Bruder, Phys. Rev. B **70**, 125305 (2004).
[14]M. Arif, D. E. Brown, G. L. Greene, R. Clothier, and K. Littrell, Vib. Monit. Control **2264**, 20 (1994).
[15]C. Shahi, M. Arif, D. Cory, T. Mineeva, J. Nsofini, D. Sarenac, C. Williams, M. Huber, and D. Pushin, Nucl. Instrum. Methods Phys. Res., Sect. A **813**, 111 (2016).
[16]D. A. Pushin, M. G. Huber, M. Arif, C. B. Shahi, J. Nsofini, C. J. Wood, D. Sarenac, and D. G. Cory, Adv. High Energy Phys. **2015**, 687480 (2015).
[17]P. Saggu, T. Mineeva, M. Arif, D. G. Cory, R. Haun, B. Heacock, M. G. Huber, K. Li, J. Nsofini, D. Sarenac, C. B. Shahi, V. Skavysh, W. M. Snow, S. A. Werner, A. R. Young, and D. A. Pushin, Rev. Sci. Instrum. **87**, 123507 (2016).

[18]D. A. Pushin, M. Arif, and D. G. Cory, Phys. Rev. **79**, 053635 (2009).
[19]D. Pushin, M. Huber, M. Arif, and D. Cory, Phys. Rev. Lett. **107**, 150401 (2011).
[20]H. Lemmel, Phys. Rev. B **76**, 144305 (2007).
[21]J. Springer, M. Zawisky, H. Lemmel, and M. Suda, Acta Crystallogr., Sect. A **66**, 17 (2010).
[22]M. Zawisky, J. Springer, and H. Lemmel, Nucl. Instrum. Methods Phys. Res., Sect. A **634**, S46 (2011).
[23]H. Lemmel, Acta Crystallogr., Sect. A **69**, 459 (2013).
[24]T. Potocar, M. Zawisky, H. Lemmel, J. Springer, and M. Suda, Acta Crystallogr., Sect. A **71**, 534 (2015).
[25]A. Ioffe and M. Vrana, Appl. Phys. A **74**, s314 (2002).
[26]F. Wiedtfeldt, M. Huber, T. Black, H. Kaiser, M. Arif, D. Jacobson, and S. Werner, Physica B **385–386**, 1374 (2006).
[27]G. L. Greene and V. Gudkov, Phys. Rev. C **75**, 015501 (2007).
[28]H. Lemmel and A. G. Wagh, Phys. Rev. A **82**, 033626 (2010).
[29]D. Petrascheck and R. Folk, Phys. Status Solidi **36**, 147 (1976).
[30]D. A. Pushin, M. Arif, M. G. Huber, and D. G. Cory, Phys. Rev. Lett. **100**, 250404 (2008).
[31]D. Petrascheck, Phys. Rev. B **35**, 6549 (1987).
[32]H. Rauch, H. Wolwitsch, H. Kaiser, R. Clothier, and S. A. Werner, Phys. Rev. A **53**, 902 (1996).
[33]E. Wolf, *Theory of Coherence and Polarization of Light* (Cambridge Press, Cambridge, 2007).
[34]J. Nsofini, K. Ghofrani, D. Sarenac, D. G. Cory, and D. A. Pushin, Phys. Rev. A **94**, 062311 (2016).
[35]N. F. Ramsey, Phys. Rev. **78**, 695 (1950).
[36]R. J. Glauber, Phys. Rev. **130**, 2529 (1963).
[37]A. Zeilinger, Am. J. Phys. **49**, 882 (1981).
[38]W. H. Zachariasen, *Theory of X-ray Diffraction in Crystals* (Wiley, New York, 1945).
[39]H. Rauch and D. Petrascheck, Top. Curr. Phys. **6**, 303 (1978).
[40]V. F. Sears, *An Introduction to the Theory of Neutron Optical Phenomena and Their Applications* (Oxford University Press, New York, 1989).
[41]U. Bonse and W. Graeff, *X-ray and Neutron Interferometry* (Springer, Heidelberg, 1977).
[42]B. W. Batterman and H. Cole, Rev. Mod. Phys. **36**, 681 (1964).
[43]A. Authier, *Dynamical Theory of X-ray Diffraction* (Oxford University Press, Oxford, 2006).
[44]E. L. Hahn, Phys. Rev. **80**, 580 (1950).
[45]U. Bonse and H. Rauch, *Neutron Interferometry* (Oxford University Press, Oxford, UK, 1979).
[46]M. G. Huber, "Thesis precision measurement of neutron interaction with matter," Ph.D. thesis (Tulane University, 2008).
[47]E. D. Becker, J. A. Feretti, and T. C. Farrar, J. Am. Chem. Soc. **91**, 7784 (1969).
[48]H. Y. Carr and E. M. Purcell, Phys. Rev. **94**, 630 (1954).
[49]K. Bongs, S. Burger, S. Dettmer, D. Hellweg, J. Arlt, W. Ertmer, and K. Sengstock, Phys. Rev. A **63**, 031602 (2001).
[50]D. Petrascheck and H. Rauch, Acta Cryst. **A40**, 445 (1984).
[51]D. A. Pushin, "Coherent control of neutron interferometry," Ph.D. thesis (MIT, 2006).